Available online at www.sciencedirect.com

SciVerse ScienceDirect

Journal of the European Ceramic Society 32 (2012) 2311–2316

www.elsevier.com/locate/jeurceramsoc

Densification and enhancement of the grain boundary conductivity of gadolinium-doped barium cerate by ultra fast flash grain welding

R. Muccillo [a,*], E.N.S. Muccillo [a], M. Kleitz [b]

[a] *Center of Science and Technology of Materials, Energy and Nuclear Research Institute, Travessa R 400, Cidade Universitaria, Sao Paulo, SP 05508-900, Brazil*
[b] *Laboratory of Electrochemistry and Physicochemistry of Materials and Interfaces - LEPMI, Polytechnique Institute of Grenoble - INPG, 1130 Rue de la Piscine, BP 75, 38402 St. Martin d'Hères, France*

Received 27 October 2011; received in revised form 16 January 2012; accepted 27 January 2012
Available online 4 March 2012

Abstract

Doped barium cerate is a promising solid electrolyte for intermediate temperature fuel cells as a protonic conductor. However, it is difficult to sinter it to high density at a reasonable temperature. Moreover, it presents a high grain boundary resistivity at intermediate temperatures. Flash grain welding was applied to compacted samples, starting from a temperature of 910 °C and applying, for a short time, an ac electric polarization of 40 V, 1000 Hz. At that frequency, the resulting current flows through the grain boundaries promoting a welding via a local Joule heating. A large decrease of the grain boundary resistivity was observed by impedance spectroscopy. Scanning electron microscopy observations of polished and etched surfaces revealed highly sintered regions. Attempts were also made to combine flash grain welding with conventional sintering.
© 2012 Elsevier Ltd. All rights reserved.

Keywords: A. Sintering; B. Grain boundaries; C. Impedance; Flash grain welding

1. Introduction

Solid electrolytes having higher ionic conductivity than that of yttria-stabilized zirconia (YSZ) in the intermediate temperature (IT) range 600–800 °C would improve the operating conditions of the solid oxide fuel cells (SOFC).[1–4]

Various compounds have been proposed, as electrolytes, including GDC and SDC (Gd- and Sm-doped cerium oxide),[5,6] BiMEVOX (Bi metal vanadium oxides),[7] and LSGM (doped lanthanum gallates),[8] all of them with an oxide ion conductivity higher than that of YSZ at intermediate temperature. Currently, peculiar drawbacks complicate their implementations. Doped cerias undergo a partial reduction, inducing an additional electronic conduction in contact with the anodic atmospheres; BiMEVOXs show structural phase transitions preventing their stabilization in the high conductivity structure; and in LSGM, secondary phases precipitate at the grain boundaries, reducing the material conductivity. Protonic conductors such as yttrium or rare earth-doped barium cerates and zirconates[9] are potential alternatives. The main advantage of proton conduction is the generation of the combustion product, H_2O, on the air side. This prevents the dilution of the combustible by this gas, a common technical problem with the oxide ion conductors.[10] The barium cerate-based ceramic proton conductors also have their own problems to be solved, such as a chemical instability under water vapor.[11–14] High sintering temperatures are also required to obtain dense materials and the high grain boundary resistivity seriously limits their performances.[15] The use of sintering aids allows a lowering of the sintering temperatures[16–31] but without alleviating the grain boundary problem.

Several alternatives to the conventional sintering of green compacts composed of nanosize particles have been proposed, in the search for better mechanical and electrical properties associated with higher density and smaller average grain size. One of these, called SPS (spark plasma sintering), or electric current assisted/activated sintering (ECAS) or field activated sintering technique (FAST), promotes densification by the simultaneous action of a high direct current through graphite dies and uniaxial pressure. Very high heating rates are reached. SPS has been widely used for the sintering of ceramic oxides.[32,33] Enhanced sintering rate and finer grain size were also obtained in yttria-stabilized zirconias[34–44] under a simple dc polarization.

* Corresponding author. Tel.: +55 11 31339203; fax: +55 11 31339276.
E-mail address: muccillo@usp.br (R. Muccillo).

0955-2219/$ – see front matter © 2012 Elsevier Ltd. All rights reserved.
doi:10.1016/j.jeurceramsoc.2012.01.032

A detailed account of the differences between "flash sintering" and "field assisted sintering" has been reported.[41] The former method occurs at low temperatures and high electric fields while the latter occurs at high temperatures reached at high heating rates and low electric fields. Very recently a single phase and highly dense 10 mol% Y-doped barium zirconate pellet was obtained by SPS, with a 5 min dwell at 1700 °C.[45]

Recent results obtained by flash grain welding (FGW) on YSZ[46] suggest that the technique could also tackle simultaneously both problems found in the preparation of doped barium zirconates: enhancement of densification and decrease of the grain boundary resistivity.

The flash grain welding technique consists, basically, in passing an ac current through a compacted green body heated to a temperature sufficient for the material to become an electrical conductor. Choosing suitable frequencies enables heat dissipation at the grain boundaries. This technique is here applied for the first time to Gd-doped barium cerate compounds.

2. Experimental

$BaCe_{0.8}Gd_{0.2}O_{3-\delta}$ ceramic powders were synthesized by mixing thoroughly, in an agate mortar, stoichiometric amounts of barium carbonate, cerium oxide and gadolinium oxide, all from Alfa Aesar, and calcining three times the mixture at 1250 °C for 15 h with intermediate attrition millings. X-ray diffraction measurements carried out on the powder ascertain that the calcination and grinding steps were sufficient for attaining the expected perovskite phase.

Before pressing into pellets, the ceramic powders were further comminuted in a homemade attritor with a ptfe-lined stainless steel container, ptfe blades, and 1 mm diameter 3Y-TZP Tosoh grinding medium immersed in isopropanol. The attrition was carried out four short times with 15 min intervals for avoiding particle neck formation due to local heating. The powders were then uniaxially pressed under 30 MPa and then isostatically under 200 MPa. The green density was in the 35–40% range (2.2–2.5 g/cm^3). Typical dimensions of the green pellets were 5.0 mm in diameter and 4.5 mm thickness.

For the flash grain welding experiments, the green pellets had their parallel bases painted with platinum paste (Degussa 308A) and were heat treated at approximately 500 °C for elimination of the organic solvent.

Basically, the flash grain welding setup is composed of a sample chamber described in detail elsewhere,[46] a furnace, a homemade power supply (0–62 V, 1000 Hz) and a data logger for collecting simultaneously the applied voltage and current versus time.

A FGW experiment consists in: (a) placing the ceramic specimen (either green or pre-sintered as described below) between two platinum meshes, connected, via Pt–Ir wires, to the power supply or to a Hewlett Packard 4192A impedance analyzer; (b) heating up the sample to a temperature T_Z and collect the impedance data. The temperature T_Z is chosen such that the impedance plot covers the frequency range of both the grains and the grain boundaries. For most of our experiments, it is about 525 °C; (c) heating to a suitable "start" temperature of approximately 910 °C where the sample resistance is of about 10 Ohms and then apply the FGW ac voltage; (d) turning off the ac voltage as soon as the flash occurs. Otherwise an avalanche current could melt the specimen (with some commercial power supplies a threshold limiting current can be set to control this current runaway); (e) cooling down to T_Z to collect again the impedance data to be compared to the pre-FGW ones.

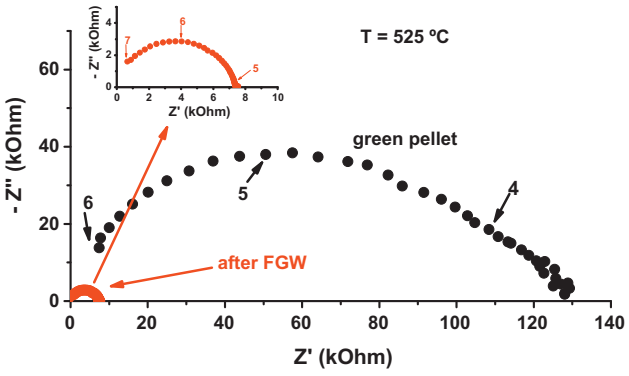

Fig. 1. Impedance plots of $BaCe_{0.8}Gd_{0.2}O_{3-\delta}$ recorded at 525 °C before and after a flash grain welding starting at 910 °C. The inset shows a zoom of the impedance plot after flash grain welding. The numbers near the arrows stand for welding the logarithm of the frequency (Hz).

Besides the conventional FGW experiments described above, FGW on a pellet pre-sintered at 1600 °C was carried out and also a further sintering at 1600 °C of a pellet already flash grain welded.

For collecting and analyzing the impedance plots in the 10 Hz to 10 MHz frequency range, a special software was used, allowing the deconvolution of the grain and grain boundary semicircles.[47,48]

Scanning electron microscopy observations were carried out in a Philips XL 30 microscope on polished (SiC and diamond polishing media down to 1 μm) and thermally etched surfaces.

3. Results and discussion

3.1. Flash grain welding of green pellets

Fig. 1 compares the impedance diagrams of $BaCe_{0.8}Gd_{0.2}O_{3-\delta}$ (BCGd) before and after FGW. The 40 V, 1000 Hz flash lasted 5 s. The flash profile is shown in Fig. 2. The maximum current is 2.7 A and the duration at half-width, 2 s. It is important to emphasize that with the ac pulse no overall mass transport occurs. The blackening effect, known to occur in zirconia upon dc bias at high temperatures, due to reduction of the specimen, is not observed here.

The impedance plot of the green pellet is typical of a porous specimen apparently with two overlapping semicircles: the high frequency one for $\log f > \sim 4$ (bulk) and the low frequency one for $\log f < \sim 4$ (interfaces = grain boundary + pores). The effect of the ac current pulse is evident. The electrical resistance after FGW decreases from 130 kOhm to 7.5 kOhm. An estimate of the capacitances of the two responses may be done, assuming an equivalent circuit composed of a resistance in parallel with a capacitance. The capacitances were evaluated taking the

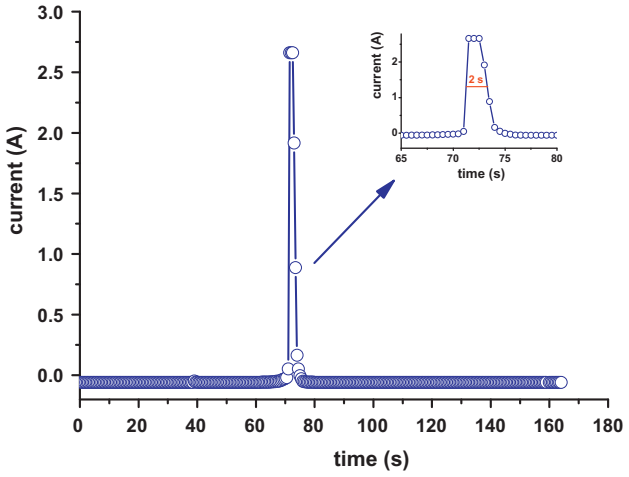

Fig. 2. Current flash across a $BaCe_{0.8}Gd_{0.2}O_{3-\delta}$ green pellet during application of 40 V, 1000 Hz at 910 °C. Inset: zoom showing a 2 s half-width.

value of the frequency at the apex of the semicircles and making use of the usual relationship $\omega RC = 1$. After the FGW procedure, only the semicircle for $\log f > \sim 5$ remains, evidencing that the current flash welded the grains, reducing drastically the blocking of charge carriers. Capacitance values, C_{HF}, of about 1.0×10^{-11} F and 1.6×10^{-11} F were obtained for the high frequency semicircle, respectively, before and after FGW. Before the FGW, an estimate of the capacitance of the interface yields $C_{LF} = 1.3 \times 10^{-9}$ F, typical of grain boundaries. These values are of the same order of magnitude as those already reported for the "bulk" response ($C_{bulk} = 10^{-11}$ F and $C_{gb} = 10^{-9}$ F,[49] $C_{bulk} = 4 \times 10^{-11}$ F and $C_{gb} = 5 \times 10^{-9}$ F[45]).

The microstructures of $BaCe_{0.8}Gd_{0.2}O_{3-\delta}$ specimens after a thermal cycle to 910 °C without FGW (blank experiment) and after FGW are shown in Fig. 3a and b (blank) and Fig. 3c and d (FGW). The image in Fig. 3a shows a porous microstructure. For this relatively low curing temperature, it can be observed that a slight sintering has started and that some grains are being structured (Fig. 3b, higher magnification). After FGW (Fig. 3c and d), the specimen shows a duplex-type microstructure with dense and porous regions, indicating that the FGW proceeded along a preferential path, probably related to a heterogeneous packing of the particles. Fig. 3c shows the dense region. The microstructure is highly homogeneous. Even though the thermal etching at 1200 °C/20 min was not sufficient for clearly delineating the grains, a segregation of small spheroid particles are seen at the grain boundaries and give an acceptable definition of the polygonal grain boundaries. These precipitated particles might be yttrium oxide.[20,50] The structured grains have different sizes, larger than 1 μm. After FGW the evaluated geometrical density is ~5.2 g/cm^3 (~84% of the theoretical density). The green density was 48% TD.

A further confirmation of the flash localization can be found in holes on the specimen surface. Focusing the observation inside the holes (Fig. 3d) reveals a dense region with welded grain boundaries.

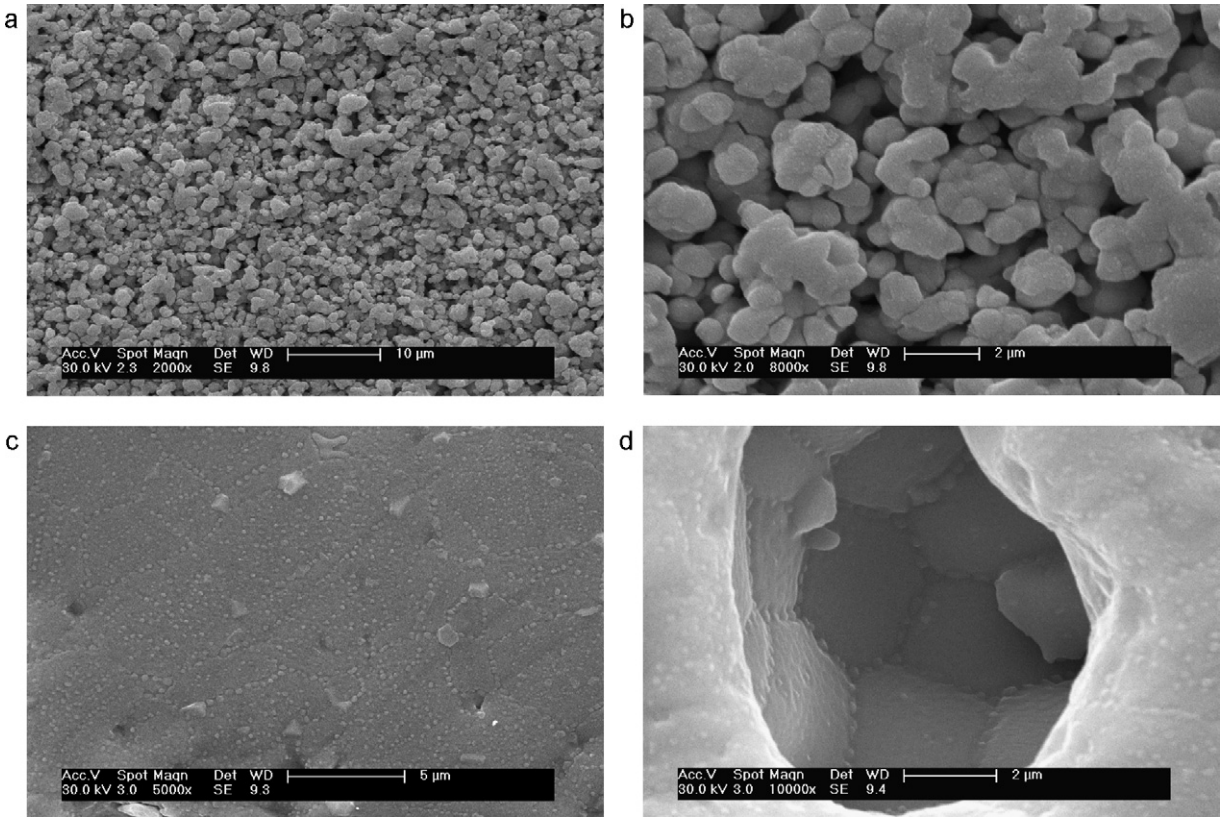

Fig. 3. (a and b) SEM micrographs of $BaCe_{0.8}Gd_{0.2}O_{3-\delta}$ just heated to 910 °C (blank specimen) with different magnifications; (c and d) after flash grain welding: (c) overall picture; (d) inside of open surface holes.

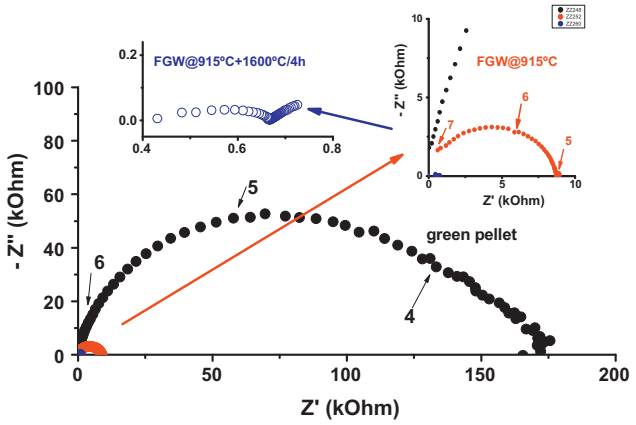

Fig. 4. Impedance plots at 525 °C of $BaCe_{0.8}Gd_{0.2}O_{3-\delta}$ before flash grain welding, after flash grain welding, and after further sintering at 1600 °C/4 h. Insets: right, zooming on the 0–12 Ohm zone; left, on the 0–0.8 Ohm zone. The numbers near the arrows stand for the logarithm of the frequency (Hz).

3.2. Sintering before and after flash grain welding

Pre-sintering and post-sintering effects on the flash grain welding were also investigated. In the pre-sintering experiment, a green specimen was initially sintered at 1600 °C, 4 h. Its impedance plot was taken at 525 °C. Then it was regularly flashed as described above and its impedance plotted again at 525 °C. In the post-sintering experiment, a green specimen was regularly flash grain welded and had its impedance plot taken at 525 °C. Then it was sintered at 1600 °C, 4 h. The idea was to see whether the improvement of the grain contact by the flash grain welding would improve a conventional densification, which occurs via mass transport around the grain boundaries.

The impedance plots of post-sintered and pre-sintered specimens are shown in Figs. 4 and 5, respectively. The green pellets show an overall electrical resistance of about 175 kOhm at 525 °C (green pellets slightly different in geometrical factors have slightly different resistances). After FGW, the electrical resistance measured at 525 °C is drastically reduced (∼20 times) to ∼9 kOhm. Post-sintering promotes a further reduction (∼10 times) of the electrical resistance to ∼0.7 kOhm. Then, the diagram allows an unambiguous separation of the grain and intergrain responses. We would conclude from this observation that the applied ac field does weld the grains. However, as the pulse is very short (∼2 s) the generated heat is not enough to really sinter them. A further sintering appears to be promoted by the presence of necks generated by the welding.

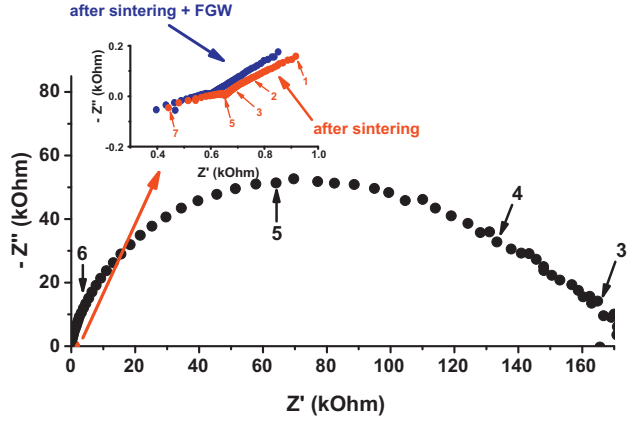

Fig. 5. Impedance plots at 525 °C of $BaCe_{0.8}Gd_{0.2}O_{3-\delta}$ after sintering at 1600 °C/4 h and after a further flash grain welding. Inset: zoom on the 0–1 Ohm zone. The numbers near the arrows stand for the logarithm of the frequency (Hz).

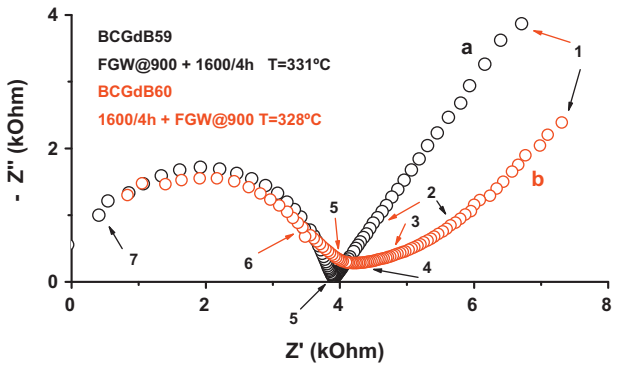

Fig. 6. Impedance plots of $BaCe_{0.8}Gd_{0.2}O_{3-\delta}$ with flash grain welding after (a) and before (b) sintering at 1600 °C/4 h. The numbers near the arrows stand for the logarithm of the frequency (Hz).

The impedance diagrams before and after the subsequent FGW (Fig. 5), in the *post*-FGW experiment, demonstrate that FGW does not result in any significant improvement (see inset of Fig. 5). This comparison points out a major feature: the physical property implemented in the FGW is associated to crude contacts between the grains. As soon as they are sintered, in other words, as soon as the grains are linked by necks, the material behaves as a simple electrical resistor and the passing of a current induces a Joule effect more uniformly distributed.

Impedance plots were also recorded at temperatures close to 330 °C for a better resolution of the grain responses (Fig. 6). The responses of the samples submitted to a priori and a posteriori FGW indicate that there is not a large difference in the intragranular resistances which are of the order of 4 kOhm. This allows us to conclude that the densification is about the same in both cases.[51]

4. Conclusions

The application at a relatively low temperature (910 °C) of 40 Vac to gadolinium-doped barium cerate polycrystalline ceramics in the green state promotes a large increase of the grain boundary conductivity as well as sintering of a part of the sample along the current passway. Even though a more detailed electron microscopy analysis is required to characterize what happens in the intergranular welded zone, this experimental procedure opens a way for obtaining high proton conductivity barium compounds under simple laboratory conditions, by the decrease of the charge carrier blocking at the grain boundaries. More experiments are also needed to improve the densification homogeneity.

Acknowledgement

To FAPESP (Proc. 05/53241-9 for financial support and Proc. 2010/51293-0 for Prof. M. Kleitz stay in Brazil).

References

1. Yokokawa H, Sakai N, Horita T, Yamaji K, Brito ME. Solid oxide electrolytes for high temperature fuel cells. *Electrochemistry* 2005;**73**:20.
2. Hibino T, Hashimoto A, Suzuki M, Sano M. A solid oxide fuel cell using Y-doped $BaCeO_3$ with Pd-loaded FeO anode and $Ba_{0.5}Pr_{0.54}CoO_3$ cathode at low temperatures. *J Electrochem Soc* 2002;**149**:A1503.
3. Ito N, Iijima M, Kimura K, Iguchi S. New intermediate temperature fuel cell with ultra-thin proton conductor electrolyte. *J Power Sources* 2005;**152**:200.
4. Matsumoto H, Nomura I, Okada S, Ishihara T. Intermediate-temperature solid oxide fuel cells using perovskite-type oxide based on barium cerate. *Solid State Ionics* 2008;**179**:1486.
5. Steele BCH. Appraisal of $Ce_{1-y}Gd_yO_{2-y/2}$ electrolytes for IT-SOFC operation at 500 °C. *Solid State Ionics* 2000;**129**:95.
6. Jurado JR. Present several items on ceria-based ceramic electrolytes: synthesis, additive effects, reactivity and electrochemical behavior. *J Mater Sci* 2001;**36**:1133.
7. Abraham F, Boivin JC, Mairesse G, Nowogrocki G. The BIMEVOX series—a new family of high performances oxide ion conductors. *Solid State Ionics* 1990;**40**:934.
8. Ishihara T, Furutani H, Yamada T, Takita Y. Oxide ion conductivity of double doped lanthanum gallate perovskite type oxide. *Ionics* 1997;**3**:209.
9. Kreuer KD. Proton conductivity: materials and applications. *Chem Mater* 1996;**8**:610.
10. Taniguchi N, Hatoh K, Niikura J, Gamo T, Iwahara H. Proton conductivity properties of gadolinium-doped barium cerates at high temperatures. *Solid State Ionics* 1992;**53**:998.
11. Scholten MJ, Schoonman J, van Miltenburg JC, Oonk HAJ. Synthesis of strontium and barium cerate and their reaction with carbon dioxide. *Solid State Ionics* 1993;**61**:83.
12. Gopalan S, Virkar AV. Thermodynamic stabilities of $SrCeO_3$ and $BaCeO_3$ using a molten salt method and galvanic cells. *J Electrochem Soc* 1993;**140**:1060.
13. Bonanos N, Knight KS, Ellis B. Perovskite solid electrolytes: structure, transport properties and fuel cell application. *Solid State Ionics* 1995;**79**:161.
14. Kreuer KD. On the development of proton conducting materials for technological application. *Solid State Ionics* 1997;**97**:1.
15. Kreuer KD. Aspects of the formation and mobility of protonic charge carriers and the stability of perovskite-type oxides. *Solid State Ionics* 1999;**125**:285.
16. Flint SD, Slade RCT. Comparison of calcium-doped barium cerate solid electrolyte prepared by different routes. *Solid State Ionics* 1995;**77**:215.
17. Chakroborty A, Das Sharma A, Maiti B, Maiti HS. Preparation of low-temperature sinterable $BaCe_{0.8}Sm_{0.2}O_3$ powder by autoignition technique. *Mater Lett* 2002;**57**:862.
18. Cai J, Laubernds K, Galasso FS, Suib SL, Liu J, Shen XF, et al. Preparation method and cation dopant effects on the particle size and properties of $BaCeO_3$ perovskites. *J Am Ceram Soc* 2005;**88**:2729.
19. Shlyakhtin OA, Orlov AV, Oh Y-J. Liquid phase low temperature sintering of niobate and cerate fine powders. *J Electroceram* 2006;**17**:405.
20. Babilo P, Uda T, Haile SM. Processing of yttrium doped barium zirconate for high proton conductivity. *J Mater Res* 2007;**22**:1322.
21. Gorbova E, Maragou V, Medvedev D, Demin A, Tsiakaras P. Influence of sintering additives of transition metals on the properties of gadolinium-doped barium cerate. *Solid State Ionics* 2008;**179**:887.
22. Gaetano C, Malavasi L, Tealdi C, Barison S, Battagliarin M, Doubova L, et al. Role of synthetic route on the transport properties of $BaCe_{1-x}Y_xO_3$ proton conductor. *J Alloys Compd* 2009;**470**:477.
23. Osman N, Talib IA, Hamid HA. Properties of sol–gel prepared $BaCeO_3$ solid electrolyte using acetate precursors. *Ionics* 2009;**15**:203.
24. Khani Z, Taillades-Jacquin M, Taillades G, Marrony M, Jones DJ, Roziere J. New synthesis of nanopowders of proton conducting materials. A route to densified proton ceramics. *J Solid State Chem* 2009;**182**:790.
25. Costa R, Grunbaum N, Berger MH, Dessemond L, Thorel A. On the use of NiO as sintering additive for $BaCe_{0.9}Y_{0.1}O_{3-\delta}$. *Solid State Ionics* 2009;**180**:891.
26. Tong JH, Clark D, Bernau L, Sandes M, O'Hayre R. Solid-state reactive sintering mechanism for large-grained yttrium-doped barium zirconate proton conducting ceramics. *J Mater Chem* 2010;**20**:6333.
27. Ricote S, Bonanos N. Enhanced sintering and conductivity study of cobalt or nickel doped solid solution of barium cerate and zirconate. *Solid State Ionics* 2010;**181**:694.
28. Souza ECC, Muccillo R. Properties and applications of perovskite proton conductors. *Mater Res* 2010;**13**:385.
29. Tong JH, Clark D, Bernau L, Subramaniyan O'Hayre R. Proton-conducting yttrium-doped barium cerate ceramics synthesized by a cost-effective solid-state reactive sintering method. *Solid State Ionics* 2010;**181**:1486.
30. Koeferstein R, Jaeger L, Ebbinghaus SB. Sintering of a fine-grained $BaCeO_3$ powder obtained from a co-precipitation method. *J Mater Sci* 2010;**45**: 6521.
31. Subramaniyan A, Tong JH, O'Hayre RP, Sammes NM. Sintering studies on 20 mol% yttrium-doped barium cerate. *J Am Ceram Soc* 2011;**94**:1800.
32. Anselmi-Tamburini U, Garay JE, Munir ZA, Tacca A, Maglia F, Spinolo G. Spark plasma sintering and characterization of bulk nanostructured fully stabilized zirconia. Part I. Densification studies. *J Mater Res* 2004;**19**:3255.
33. Anselmi-Tamburini U, Garay JE, Munir ZA, Tacca A, Maglia F, Chiodelli G, et al. Spark plasma sintering and characterization of bulk nanostructured fully stabilized zirconia. Part II. Characterization studies. *J Mater Res* 2004;**19**:3263.
34. Ghosh S, Chokshi AH, Lee P, Raj R. A huge effect of weak dc electrical fields on grain growth in zirconia. *J Am Ceram Soc* 2009;**92**:1856.
35. Yang D, Conrad H. Enhanced sintering rate of zirconia (3Y-TZP) by application of a small AC electric field. *Scr Mater* 2010;**63**:328.
36. Yang D, Raj R, Conrad H. Enhanced sintering rate of zirconia (3Y-TZP) through the effect of a weak dc electric field on grain growth. *J Am Ceram Soc* 2010;**92**:2935.
37. Cologna M, Rashkova B, Raj R. Flash sintering of nanograin zirconia in <5 s at 850 degrees C. *J Am Ceram Soc* 2010;**93**:3556.
38. Cologna M, Raj R. Surface diffusion-controlled neck growth kinetics in early stage sintering of zirconia, with and without applied dc electrical field. *J Am Ceram Soc* 2011;**94**:391.
39. Cologna M, Prette ALG, Raj R. Flash-sintering of cubic yttria-stabilized zirconia at 750 degrees C for possible use in SOFC manufacturing. *J Am Ceram Soc* 2011;**94**:316.
40. Raj R, Cologna M, Francis JSC. Influence of externally imposed and internally generated electrical fields on grain growth, diffusional creep, sintering and related phenomena in ceramics. *J Am Ceram Soc* 2011;**94**:1941.
41. Cologna M, Francis JSC, Raj R. Field assisted and flash sintering of alumina and its relationship to conductivity and MgO-doping. *J Eur Ceram Soc* 2011;**31**:2827.
42. Yang D, Conrad H. Enhanced sintering rate and finer grain size in yttria-stabilized zirconia (3Y-TZP) with combined DC electric field and increased heating rate. *Mater Sci Eng A* 2011;**528**:1221.
43. Conrad H, Yang D. Dependence of the sintering rate and related grain size of yttria-stabilized polycrystalline zirconia (3Y-TZP) on the strength of an applied DC electric field. *Mater Sci Eng A* 2011;**528**:8523.
44. Cordier A, Kleitz M, Steil MC. Welding of yttrium-doped zirconia granules by electric current activated sintering (ECAS): protrusion formation as a possible intermediate step in the consolidation mechanism. *J Eur Ceram Soc* 2012, doi:10.1016/jeurceramsoc.2011.12.022.
45. Ricote S, Bonanos N, Wang HJ, Boukamp BA. Conductivity study of dense $BaZr_{0.9}Y_{0.1}O_{(3-\delta)}$ obtained by spark plasma sintering. *Solid State Ionics* 2012, doi:10.1016/j.ssi.2011.02.11.
46. Muccillo R, Muccillo ENS, Kleitz M. Flash grain welding in yttria stabilized zirconia. *J Eur Ceram Soc* 2011;**31**:1517.
47. Kleitz M, Kennedy JH. In: Vashishta P, Mundy JN, Shenoy GK, editors. *Fast ion transport in solids*. The Netherlands: Elsevier, North Holland; 1979. p. 185.

48. Barsoukov E, Macdonald JR. *Impedance spectroscopy—theory, experimental and applications*. 2nd ed. Wiley-Interscience; 2005.
49. Arab Pour Yazdi M, Briois P, Georges S, Shaula AL, Cavaleiro A, Billarda A. Comparison of structural and electrical properties of barium zirconate pellets and thin films. *J Electrochem Soc* 2010;**157**:B1582.
50. Muccillo R, Muccillo ENS. Synthesis and properties of $BaZr_{0.1}Ce_{0.7}Y_{0.2-x}M_xO_{3-\delta}$ ($x = 0$, 0.1; M = Dy, Yb) compounds. *ECS Trans* 2011;**31**:1251.
51. Steil MC, Thevenot F, Kleitz M. Densification of yttria stabilized zirconia. *J Electrochem Soc* 1997;**144**:390.